Tellus (1995), 47A, 779–796
Printed in Belgium – all rights reserved

TELLUS
ISSN 0280–6495

The origin and evolution of low-level potential vorticity anomalies during a case of Tasman Sea cyclogenesis

By MICHAEL J. REVELL* and ROGER N. RIDLEY, *National Institute of Water and Atmospheric Research, Ltd., P.O. Box 31311, Lower Hutt, New Zealand*

(Manuscript received 13 September 1994; in final form 21 February 1995)

ABSTRACT

The rapid development (15 hPa deepening in 12 hours) of an intense, shallow and small-scale ($\sim$300 km) cyclone off the east coast of Australia was studied, in the context of potential vorticity (PV) thinking. High-resolution spatial and temporal fields generated by a mesoscale weather prediction model, embedded within ECMWF data were used. This case was well simulated, as verified by the few available observations at neighbouring stations, and by satellite imagery. The PV distribution within this cyclone was computed from the model fields and the origin of its component parts established using backward trajectories. These indicated that at low levels the primary mechanism of PV production was the vertical gradient of latent heat release in a frontal cloud band. Above the level of maximum heating this process reversed sign with corresponding destruction of PV. As the heating became shallow enough and intense enough a low level vortex formed with a vertical scale of 2–3 km and a wave-CISK like normal mode structure. The length scale and growth rate of this mode agreed well with the observed cyclone, unlike the classical explanation for this type of development (the pure baroclinic instability mechanism of Charney and Eady) which, even including moisture, still predicts length scales of over a 1000 km and doubling times of at least a day.

1. Introduction

The Tasman Sea region is a key location for the genesis of intense winter storms in the southern hemisphere (SH). This has been demonstrated by Sinclair (1994) in a recent climatology of SH cyclones based on 6 years of ECMWF data. The high frequency of cyclones that form and reach significant intensity in this area is shown in Fig. 1, derived from this study.

A generally accepted theoretical explanation for these storms is baroclinic instability (BI), the exponential growth of small amplitude disturbances on an unstable basic state as described mathematically by both Charney (1947) and Eady (1949). These disturbances grow by converting potential energy of the basic state to kinetic and potential energy of the perturbation, through slantwise convection as explained by Green (1960). A simple conceptual model, which contains the essential features of the instabilities in Charney's and Eady's mathematical description of BI, was presented in the article by Hoskins et al. (1985), hereafter referred to as HMR. They use the dynamic variable potential vorticity (PV), defined as the three dimensional scalar product of the absolute vorticity ξ_a with the gradient of potential temperature θ, divided by the density ρ, i.e.,

$$\mathrm{PV} = \frac{1}{\rho}(\xi_a \cdot \nabla\theta),$$

to present BI as the co-operative interference of (PV) anomalies at upper and lower boundaries, where the basic state north to south gradients of PV have opposite sign. Surface potential temperature gradients at the boundary can be considered part of the interior PV distribution, since Bretherton (1966) has demonstrated their

* Corresponding author.

Fig. 1. Frequency of intense cyclone formation in the southern hemisphere. Units are cyclones per month, with contours every 0.1 units. Light shading indicates greater than 0.5 and dark shading greater than 0.7 per month.

equivalence to thin sheets of PV. If the upper and lower boundaries are considered to be the ground and the tropopause, then the resulting picture does explain some of the features of observed mid-latitude cyclones.

However, this simple model for BI has several shortcomings. Firstly, the predicted length scale and efolding time for the most unstable mode given by Eady (1949) are 6–7000 km and 2 days respectively. These are considerably larger than those generally observed. For instance Holland et al. (1987) point out some Australian "East coast lows" have scales of just a few hundred km and efolding times of a few hours. It includes no description of moist processes and their feedback on the model dynamics. Cyclones that develop in the Tasman Sea frequently produce heavy rain. For example, note the severe flooding in the Sydney area, described by Golding and Leslie (1993), during the preliminary development stage of the cyclone which is the subject of the current study.

An obvious improvement is thus to include moisture in the model description. As suggested in HMR one effect of a moist environment is to reduce the effective static stability experienced by the growing mode. The length scale of the most unstable mode scales with the Rossby radius of deformation

$$\frac{NH}{f},$$

where N is the static stability, H the depth scale (the distance between the upper and lower PV anomalies) and f the local coriolis parameter, so including moist effects will reduce this. Calculations by Emanuel et al. (1987), assuming ascending air at all levels is saturated, and conservation of equivalent potential temperature to determine the heating rate, indicate more realistic length scales of 1500 km and efolding times of 1 day are possible. In order to reduce the length scale further (assuming rotational effects are important) it appears necessary to generate PV anomalies at levels intermediate to the surface and the tropopause, thus reducing H.

As first suggested by Kleinschmidt (Eliassen and Kleinschmidt, 1957), condensational heating in the lower portions of frontal cloud masses is another source of cyclonic PV anomalies. This was noted in HMR and further emphasised by others, e.g., Reed et al. (1992) (hereafter referred to as RSK). Snyder and Lindzen (1991) in an analytical study of the feedback of organised moist convection on baroclinic waves (wave-CISK) use idealised (step function) heating profiles for condensation in an unbounded baroclinic shear zone. Mak (1994) also includes the influence of upper and lower boundaries (the Eady problem for zero heating). This work indicates that the simple explanation of BI given in HMR may be extended to include PV anomalies at intermediate levels associated with vertical gradients of latent heating.

Secondly, the assumption of simultaneous, exponential growth of small amplitude disturbances at the surface and upper levels is inconsistent with the observation of Hill (1980), that the upper level anomalies are usually of large amplitude before surface development occurs in the Tasman Sea. Synoptic and numerical studies of Australian East coast lows by Holland et al. (1987) and Leslie et al. (1987) emphasise the roles of an inhomogeneous lower boundary, surface fluxes of sensible and latent heat and without giving any detail of its distribution, diabatic heating from cumulus convection. Although not expressed in PV terms, these local studies, indicate the polar, stratospheric vortex is the source of the upper PV anomalies associated with Tasman Sea cyclogenesis. However, the origin and distribution of the low level PV anomalies is not clear. Australia, being a subtropical continent, is not capable of producing such marked land sea temperature contrasts as occur off the East coasts of the more polar continents of the northern hemisphere during winter. Moisture gradients tend to be as important as

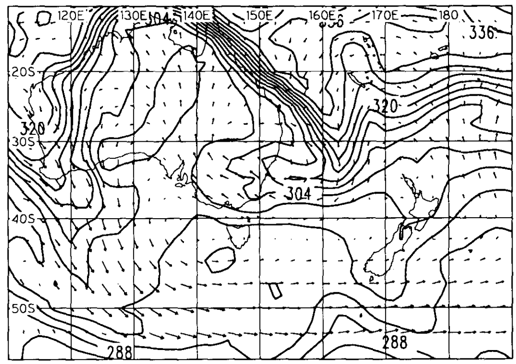

Fig. 2. ECMWF analyses of 850 hPa wind vectors and equivalent potential temperatures at 12 UTC on 1 August 1990. Contour interval 4°K and maximum wind vector 25 m s^{-1}.

temperature gradients in this region, as can be seen in Fig. 2.

Although the conceptual model of HMR explains the essence of BI, a more elaborate model is needed in order to explain these observations. This model should include the feedback on cyclone dynamics of clouds and precipitation through latent heat release and allow for the initial presence of large amplitude upper level PV anomalies. One of the purposes of this study is to build up such a model.

A schematic illustration of the PV and feedbacks for both the Eady and wave-CISK modes is contained in Fig. 3. These can be summarised as follows.

(a) Eady mode. The basic state consists of a N/S temperature gradient (vertical shear), an upper boundary N/S PV gradient due to the slope of the tropopause with latitude and a lower boundary S/N PV gradient due to surface temperature varying with latitude. The perturbation PV mode evolves according to advection of the basic state PV gradient by the induced perturbation horizontal velocities.

(b) Wave-CISK mode. The basic state contains a N/S temperature gradient but, as there are no upper or lower boundaries, no N/S PV gradients. Perturbation PV evolves according to vertical gradients of the induced latent heating. Since latent heating is proportional to vertical velocity in saturated air, a cyclonic (anticyclonic) PV anomaly is induced below (above) the level of maximum vertical velocity.

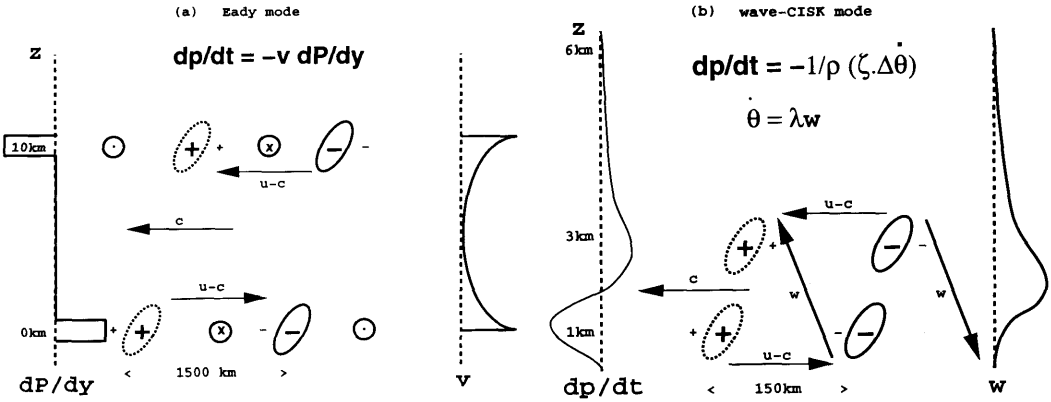

Fig. 3. Schematic diagrams of the PV and relevant feedbacks for (a) the Eady mode, (b) the wave-CISK mode. Conventions are for the southern hemisphere with circled − (+) signs indicating cyclonic (anticyclonic) PV anomalies, and small − and + signs indicating forcing from the anomaly (or vertical velocity) above or below. ⊙ and ⊗ indicate flow out of and into the paper respectively.

The vertical scale of the most unstable Eady mode h is the depth of the troposphere, typically 8 to 12 km, with horizontal scale of order Nh/f. For the wave-CISK mode the vertical scale is determined by the depth of the convection, so a range of scales is possible. For shallow convection the height and length scales could be an order of magnitude smaller. The growth rate for the wave-CISK modes is proportional to the heating rate, and could be considerably greater than for the pure Eady mode. In the real atmosphere the heating profiles are continuous and modes of both these types could interact in three dimensions. However this idealised picture is useful from a conceptual point of view, in order to appreciate similarities and differences between the many cyclones that develop. Without such conceptual models we are left with the "unsystematic details of individual cases" (Davis and Emanuel, 1991) and will make little progress towards understanding the key ingredients of the instabilities.

In this paper we present evidence of a wave-CISK like mode during the development of an Australian East coast low by numerically simulating the first of four deep storms which developed in the Tasman Sea region during the month of August 1990. We calculate the PV distribution within this rapidly deepening cyclone and with the aid of backward trajectory analyses ascertain the origin of the component parts of this PV. In particular we show that PV production (destruction) at lower (upper) levels is predominantly due to a vertical gradient of latent heat release, and that the idealised modes introduced above can explain the observed scales and growth rates.

We follow the methodology of RSK who studied a rapidly deepening marine cyclone off the east coast of the United States, but in our case use high resolution fields derived from a successful simulation of the storm using the regional atmospheric modelling system (RAMS) mesoscale model nested within gridded analyses from the European Centre for Medium range Weather Forecasts (ECMWF). We wish to establish the relative importance of the contribution of surface potential temperature anomalies, condensation in clouds, upper level vortices and their mutual interaction, to the PV evolution. As we have not yet implemented a method for inverting PV (such as described by Davis and Emanuel (1991)), this study will be limited to the calculation of PV and description of its evolution. Any arguments about mutual interaction will be restricted to relative phase and scale.

Some specific questions to be addressed in this study include:

• is there a region of warm surface thermal anomaly in the mature low?

• are surface fluxes important for storm development?

- where and how quickly is PV produced at low to middle levels by condensation?
- what triggers the transition from the gradual development to the intensification stage of the low level anomaly?
- does the large upper level PV anomaly directly influence the intense deepening stage of the storm?
- is there significant feedback of the lower level PV production through condensation on the upper level PV anomaly?

We will show the importance of moistening the lowest layers of the atmosphere by running simulations with and without surface fluxes. The importance of PV, generated by latent heating, on storm development will be demonstrated by comparing these simulations with one not including any feedback from latent heat release.

A synopsis of the paper is as follows. In Section 2, a description of the numerical model and analysis methods are presented. Section 3 provides a synoptic overview of the storm and verification of the model simulation. Trajectories and diagnostics indicating evolution of PV features during the most intense phase of development are presented in Section 4. Finally the results are discussed and summarised in Section 5.

2. Method

2.1. Model description

The model used in this study was the latest version 3a of the RAMS mesoscale model. Comprehensive technical details of this model are contained in Pielke et al. (1992). General characteristics and specific parameter settings are displayed in Table 1. The horizontal domain consisted of a rectangular grid of 65 by 50 points 40 km apart on a polar stereographic projection nested inside a similar grid of 65 by 50 points 120 km apart. There were 25 levels in the vertical terrain-following coordinate system, with the lowest full level at 50 m, seven levels below 1.5 km and the top at 20 km. The coarse grid is shown along with the sea temperatures in Fig. 4, and the fine grid along with the topography and key place names in Fig. 5. The non-hydrostatic option with a time step of 90 s was used. The non-hydrostatic option was not essential for this simulation, but many of the boundary condition options were better supported for this version of the model. An explicit moisture scheme was used retaining vapour, liquid and solid phases of water. A Kuo convective parameterisation scheme was used.

Table 1. *Model characteristics*

Data	ECMWF $2.5^\circ \times 2.5^\circ$ TOGA uninitialised, 14 level analyses
coarse domain	7800×6000 km
coarse resolution	120×120 km
fine domain	2600×2000 km
fine resolution	40×40 km
time step	90 s on both grids
orography	from global 10′ data
lower boundary	5 level soil model
physics	short/longwave radiation convective parameterisation liquid water only using default settings
diffusion	horizontal deformation vertical Mellor-Yamada

Initial atmospheric conditions were interpolated from ECMWF $2.5^\circ \times 2.5^\circ$ uninitialised TOGA analyses, available at 14 standard levels, to the model grid. Sea temperatures were obtained from NMC operational global analyses. The model runs

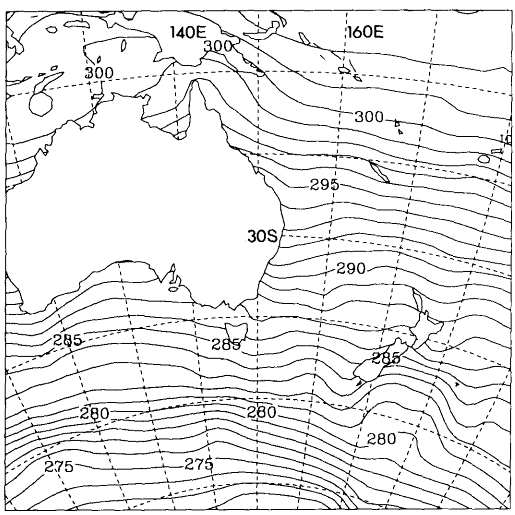

Fig. 4. August 1990 Sea Surface Temperatures in the Tasman Sea on the coarse RAMS grid. Units are °K with contours every °K.

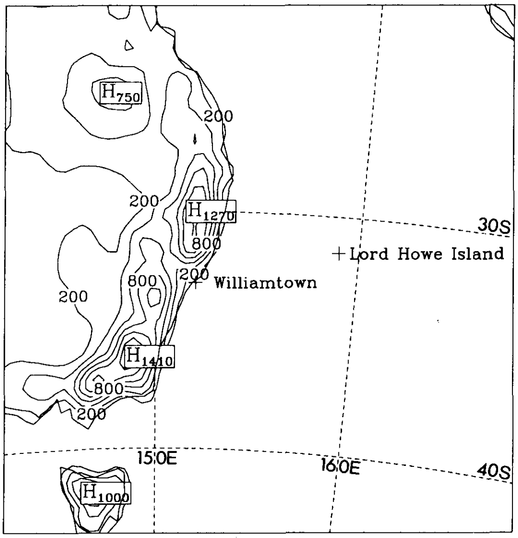

Fig. 5. Model orographic heights on the fine RAMS model grid, with the positions of Williamtown airport and Lord Howe Island marked. Units are m with contours every 200 m.

were nudged towards ECMWF 12-h analyses at the lateral and upper boundaries. A form of initialisation was performed by nudging the interior RAMS model fields moderately towards the ECMWF tendencies for the first 12 h of the integration. Subsequently the internal nudging was turned off. The simulation was run for a total period of 27 h, beginning at 00 UTC on 2 August 1990. Most rapid development was between 18 UTC on 2 August and 00 UTC on 3 August with the surface pressure falling by some 18 hPa over a 15-h period. The results presented here are mainly for the 12-h period from 12 UTC on 2 August and focus on the PV distribution at 21 UTC.

2.2. *Diagnostic methods*

Model output was analysed with the standard NCAR graphics package that comes with the RAMS model. PV (our main interest), temperature and height plots at model and isobaric levels give a comprehensive picture of the atmospheric structure at a given time. To monitor the PV evolution through the most intense development period these are supplemented with trajectory analyses and cross sections using the VIS-5D program, a MCIDAS derivative. To make use of this package all derived fields were calculated in model space before being interpolated to a regular 40 km horizontal and 500 m vertical grid.

For trajectory calculations in this study the full 40 km spatial resolution of the model was used, with 30-min time steps linearly interpolated from history files saved every hour. Some uncertainty in the accuracy of the trajectories is to be expected, especially through regions with strong gradients and vertical motion. However forward and backward trajectories along the same path showed good continuity providing confidence in the main conclusions of this study. Many trajectories were calculated of which only a small subset are presented here.

3. Synoptic overview

About 15% of cyclones developing in the shaded Tasman Sea region of Fig. 1 belong to the class of "East coast lows" according to Holland et al. (1987). They are most common in late winter and early spring. A typical development scenario is for a mid-tropospheric cold pool to become "cut off" over eastern Australia. Subsequently a trough (locally known as an "easterly dip") forms in the underlying easterly flow, intensifying as it propagates down the coast. These systems usually bring heavy rain and flooding to the east coast of Australia and occasionally develop very intense low level vortices with winds of hurricane force. Just such an event occurred during the first few days of August 1990 and is the subject of this study.

The broad scale development with time of the low level PV anomalies for this storm can be seen in the series of ECMWF analyses of PV and potential temperature at 850 hPa shown in Fig. 6. However, the fine scale details of the formation of the intense low level vortex are only captured by the RAMS model mesoscale forecasts. Both sources of information have been used to outline the storm development in the discussion which follows. This development can be divided into 3 distinct phases. Firstly, a near stationary mid to upper tropospheric cold pool (PV anomaly) formed over eastern Australia, shown at 400 hPa in Fig. 7. (Throughout the diagrams in this study, contouring of PV is in terms of PV units (PVUs) corresponding to $10^{-6}\,m^2\,s^{-1}\,K\,kg^{-1}$ following HMR and remember that cyclonic PV is negative

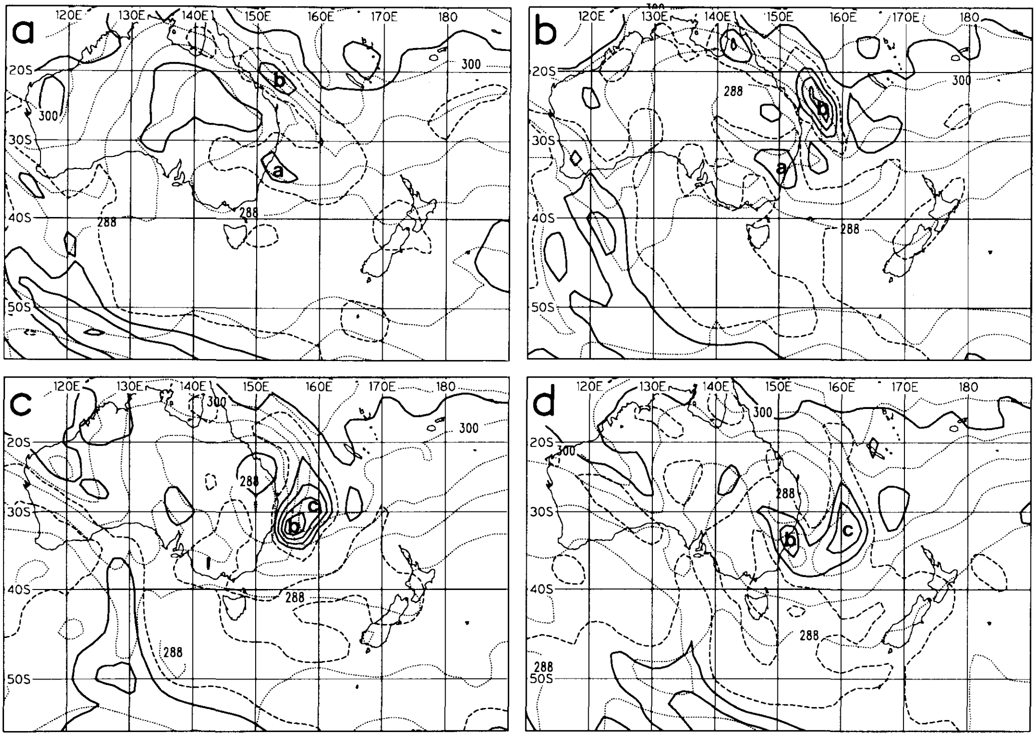

Fig. 6. ECMWF analyses of PV (solid) and θ (dotted) fields at 850 hPa (a) at 12 UTC 1 August, (b) 00 UTC 2 August, (c) 12 UTC 2 August and (d) 00 UTC 3 August 1990. PV contours are every 0.2 PVU (1 PVU $= 10^{-6}$ m^2 s^{-1} K kg^{-1}), with the -0.4 PVU contour dashed and θ contours every 4°K. Lettering corresponds to references in the text.

in the SH.) Below this, within the strengthening low level easterly flow over eastern Australia, an east coast low with weak circulation (marked "a" in Fig. 6) developed during the period 30 July to 1 August 1990. It became slow moving and produced heavy precipitation over the Sydney area as described more fully by Golding and Leslie (1993). For this system the central pressure never dropped below 1007 hPa but a cold front formed to the north and east, as shown in Fig. 2. Subsequently, from 00 UTC on 2 August a second low-level vorticity anomaly (marked "b" in Fig. 6) developed on this front, eventually replacing the first low and deepening by 15 hPa to 988 hPa at 02 UTC on 3 August. A satellite picture valid at this time is shown in Fig. 8 indicating the rather shallow and small scale nature of this system as it makes landfall on the Australian coast near Williamtown. Further evidence of the shallow but intense nature of this development is presented in the tephigram for Williamtown valid at 23 UTC on 2 August 1990 shown in Fig. 9. Note the 850 hPa winds of over 70 kts, the saturated lowest 2 km, the mixed layer between 2 and 6 km, and the dry air above 6 km are in good agreement with

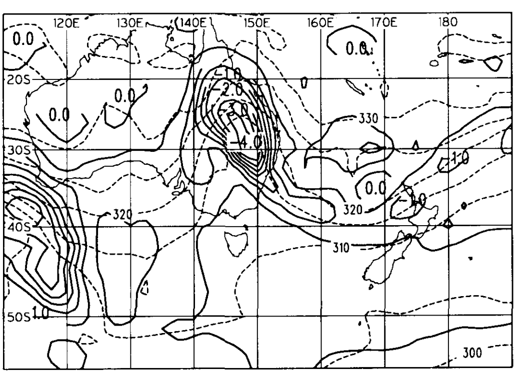

Fig. 7. ECMWF analyses of PV (solid) and θ (dashed) fields at 400 hPa at 00 UTC 2 August 1990. PV contours are every 1 PVU and θ contours every 5°K.

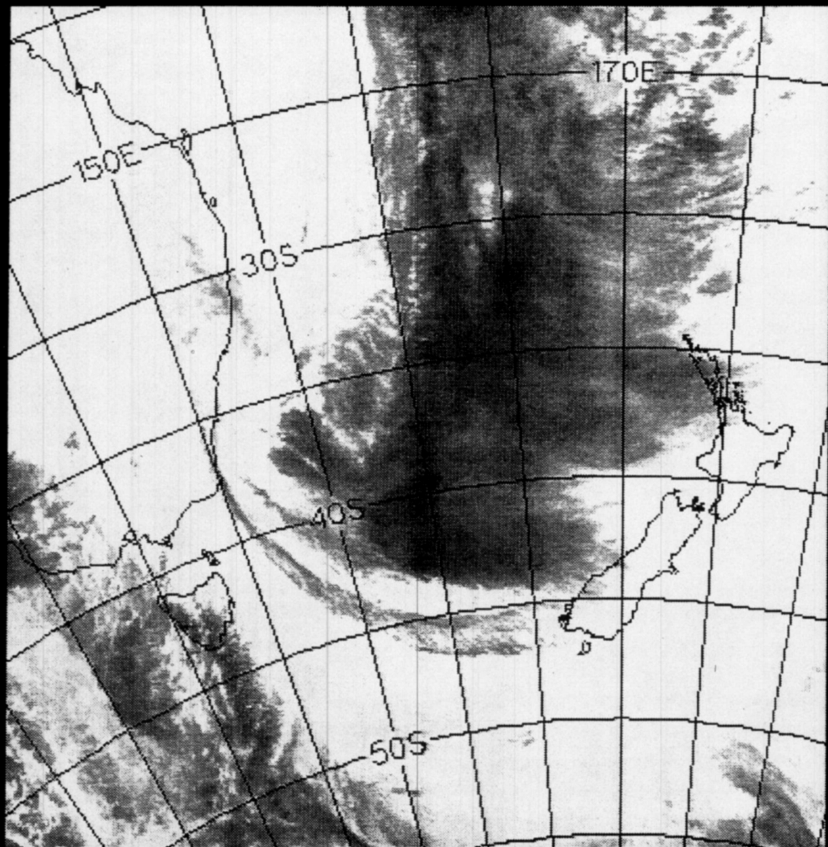

Fig. 8. Infrared geostationary satellite picture valid at 02 UTC 3 August 1990. The centre of the low level storm can be seen at (33.5° S, 152° E).

values from model trajectories to be shown later. A third low level vorticity anomaly at 32° S, 161° E (marked "c" in Fig. 6) became apparent at 00 UTC on 3 August. As this deepened the second low filled and nine hours later a ship reported an 80 kt northeasterly at 40° S, 159° E.

Studies of this type in the SH usually suffer from a shortage of standard observational data. The nearly static nature of the fields at upper levels over the (relatively) data rich Australian area during the preceding few days was a significant advantage of this case. An accurate picture of the PV fields over the Australian continent, where the upper level anomaly is located, were able to be built up over several days of analysis cycles. Surface observations however were restricted to the Australian continent and a few nearby island stations. Thus we relied heavily on the ECMWF model to get the temperature and moisture (and hence PV) fields correct to the east of Australia where low level development occurred. The only indication that the models did get this flow correct was to compare their output with observations at these island and coastal stations.

The observed and modelled surface pressures at Williamtown aerodrome and Lord Howe Island (marked by + signs in Fig. 5) are shown in Fig. 10 over this period. The model simulated the observed mean sea level pressure trace at Williamtown aerodrome well. At Lord Howe island agreement

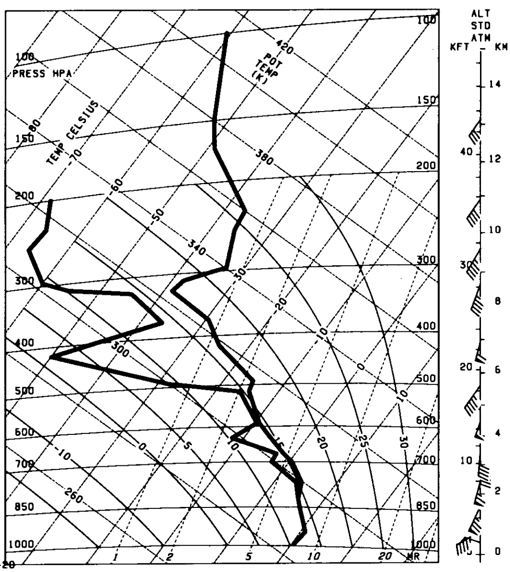

Fig. 9. Tephigram for Williamtown airport, valid at 23 UTC 2 August 1990.

was not so good, mainly because the model tended to over deepen the whole system to the East of Australia by 3–4 hPa, particularly during the third phase. However, the feature of main interest, the shallow, second stage low level development was well simulated.

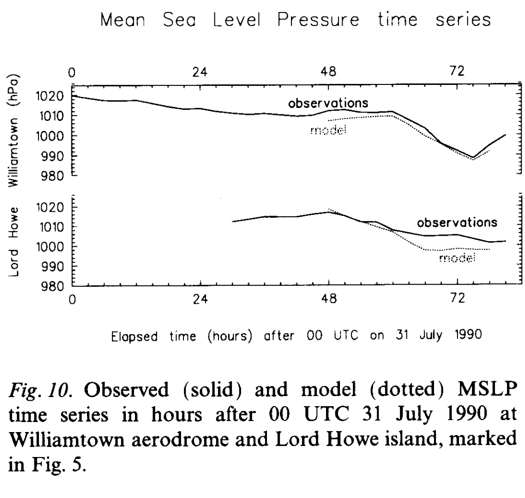

Fig. 10. Observed (solid) and model (dotted) MSLP time series in hours after 00 UTC 31 July 1990 at Williamtown aerodrome and Lord Howe island, marked in Fig. 5.

4. PV evolution

As shown in Section 3, the model simulation produced an accurate simulation of the storm during its second stage giving us confidence in its suitability for examining the PV evolution. We focus primarily on the PV distribution at 21 UTC, 2 August in the vicinity of the low level development using individual backward trajectories to indicate the origin of PV features. Model generated PV fields are presented in cross sections and constant height surfaces. Traditionally PV has been presented on isentropic surfaces, but we can calculate it just as accurately on model surfaces (without the need for extra interpolation). Also the advantage of being able to advect PV along isentropic surfaces is negligible in this case for as we will show diabatic effects dominated.

As in RSK we will qualitatively refer to isolated PV features as anomalies, although strictly speaking a PV anomaly refers (as pointed out in HMR) to the PV deviation from a reference value on the particular isentropic surface in question. We are confident the features referred to as anomalies would stand up to a more rigorous definition.

4.1. *Surface temperature anomaly*

In this Subsection we consider surface trajectories between 00 and 21 UTC on 2 August which finish around the pressure and PV centres. These are shown in Fig. 11, superimposed on top of the surface temperature anomaly at the latter time, with P and L indicating the potential vorticity and pressure centres respectively. Following RSK this anomaly represents the departure from the time mean over the period 00 UTC 2 August to 06 UTC 3 August. Light (medium) shading corresponds to positive (negative) temperature anomalies. A small positive anomaly, with maximum just over 1.5°C is located just south and east of the developing low level PV centre. Table 2 shows the variables height (h), relative humidity (RH), potential temperature (θ), pseudo wetbulb potential temperature (θ_e), PV and pressure (p) along the respective trajectories. The model sea surface θ is approximately 290°K at the centre of the surface low at 21 UTC.

Trajectories generally remained close to the surface and changes in the values can be attributed to surface fluxes, except between 00 and 12 UTC when nudging towards ECMWF tendencies took place. From a Lagrangian viewpoint the diabatic

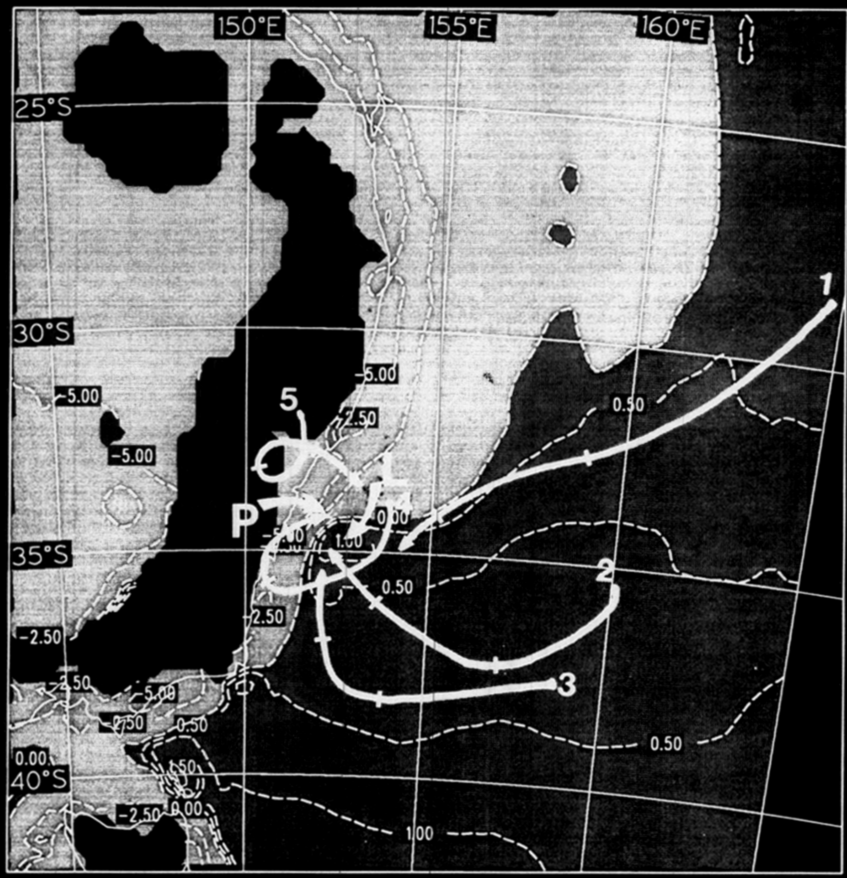

Fig. 11. RAMS model derived surface trajectories between 00 and 21 UTC on 2 August 1990. *P* and *L* correspond to the PV and pressure centres respectively. Trajectories start at the corresponding number given in Table 2, with crosses indicating intermediate times. Light (medium) shading corresponds to positive (negative) surface potential temperature anomalies. Units are °K with positive (negative) contours every 0.5 (2.5)°K. White shading corresponds to orographic heights greater than 200 m.

contribution can be obtained by taking the difference between the initial and final values along a trajectory. For trajectory 1 which originated in the warm moist air to the northeast, air-sea interaction diminished the magnitude of both θ and θ_e over a shallow layer. For trajectories 2 and 3 originating in cooler air, air-sea interaction has an enhancing effect of 1–2°C. Trajectories 4 and 5 eventually descend from over the land ahead of the advancing low, with both θ and θ_e rising by 4°C in the process. This indicates a significant surface flux of latent heat over 3 h.

In order to get an appreciation of the distribution of surface fluxes relative to the developing storm, surface sensible and latent heat fluxes are shown in Fig. 12 as calulated by the RAMS model at 21 UTC on 2 August. As expected these are roughly proportional to the wind speed. In the strong northeasterly flow to the east of the cold front (east of 160° E and north of 35° S) sensible heat flux is negative (warm air over colder ocean) but latent heat flux is quite strongly positive (over 150 W m^{2}). The other region of interest is in the strong offshore flow ahead of the advancing storm, just off the east coast of Australia, where cold dry air is being advected rapidly over a relatively warm

Table 2. *Values of h, RH, θ, θ_e, PV and p along the surface trajectories in Fig. 11 (units are km, %, °K, °C, PVU and hPa, respectively)*

No.	Time	h	RH	θ	θ_e	PV	p
1	00/2	0.08	81.0	291.8	17.0	−0.04	1011.0
	12/2	0.08	96.1	291.1	17.5	−0.27	991.1
	18/2	0.08	89.8	290.6	16.7	−0.29	982.1
	21/2	0.08	90.8	290.0	16.3	−0.19	980.8
2	00/2	0.08	89.6	289.6	15.7	−0.16	1009.1
	12/2	0.08	99.1	288.3	14.3	−0.14	1005.1
	18/2	0.08	94.5	290.0	15.7	−0.38	983.5
	21/2	0.08	94.7	291.1	16.4	−0.39	978.4
3	00/2	0.08	88.3	287.3	13.5	−0.23	1008.6
	12/2	0.08	85.5	287.7	13.5	−0.13	1002.9
	18/2	0.08	95.3	288.1	14.0	−0.13	990.8
	21/2	0.08	95.3	289.2	14.6	−0.39	980.2
4	00/2	0.17	66.2	290.0	12.7	−0.25	989.8
	12/2	0.39	91.6	287.1	11.7	−0.25	962.5
	18/2	0.17	98.5	284.2	10.4	−0.10	971.5
	21/2	0.08	95.9	287.4	13.1	−0.57	979.0
5	00/2	0.77	77.8	288.2	9.9	−0.62	916.8
	12/2	0.64	94.3	284.9	8.9	−0.38	934.0
	18/2	0.34	91.2	281.8	7.4	−0.46	954.7
	21/2	0.08	90.7	286.4	11.7	−0.19	982.4

ocean. Here values of 400 W m^2 for sensible heat flux and 550 W m^2 for latent heat flux can be seen near the coast.

The impact of these surface fluxes on storm depth is shown in Table 3. Removing all surface

Table 3. *Central pressure (hPa) and low position (lat S, lon E) of (a) analyses and model runs with (b) full physics, (c) no surface fluxes and (d) no latent heating*

Experiment	Time	Position	Central pressure
(a)	12/2	(−30.0, 158.0)	1004.0
	18/2	(−34.0, 153.5)	995.6
	00/3	(−33.5, 152.5)	989.3
(b)	12/2	(−31.5, 157.4)	1003.0
	18/2	(−34.3, 153.5)	993.2
	00/3	(−33.7, 152.4)	990.1
(c)	12/2	(−31.5, 157.4)	1003.0
	18/2	(−34.5, 153.5)	993.9
	00/3	(−34.0, 152.5)	991.1
(d)	12/2	(−31.5, 157.4)	1003.0
	18/2	(−33.0, 155.0)	998.0
	00/3	(−34.5, 154.0)	996.3

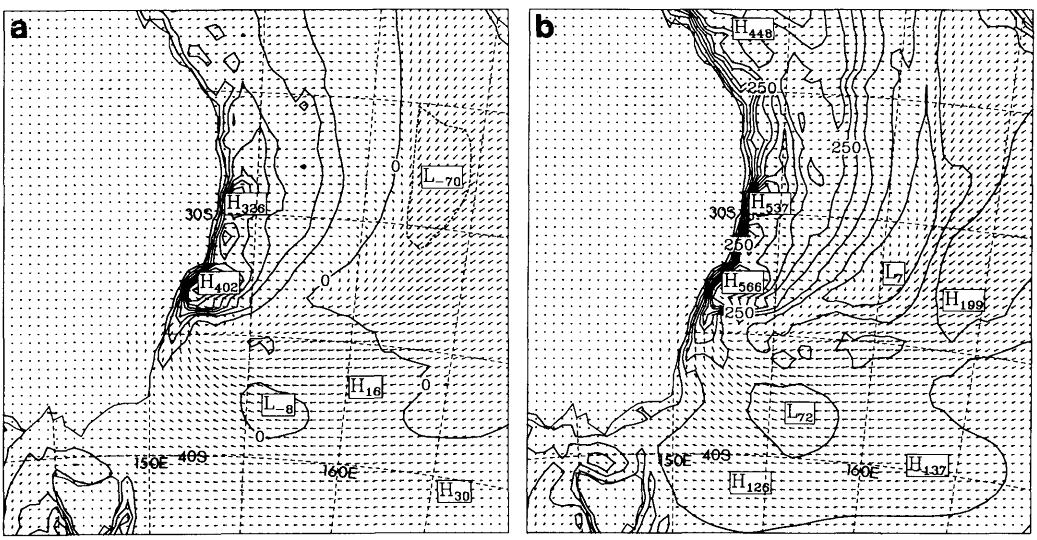

Fig. 12. RAMS model derived surface fluxes in W m^{-2} at 21 UTC on 2 August 1990, of (a) sensible and (b) latent heat. Contours in (a) every 40 W m^{-2} and in (b) every 50 W m^{-2}. Wind vectors at the lowest model level of 25 m are also shown. A vector equal to the grid spacing corresponds to 25 m s^{-1}.

fluxes has about a 10% influence on the minimum storm pressure, and slightly inhibits the approach of the storm towards the coast. Thus the surface fluxes seem to play a relatively minor role in the direct development of this storm, however they appear to be important for preconditioning the low level air to be warm and moist enough for the wavelike instability, detailed in the next section, to occur. Given its small magnitude the surface thermal anomaly appears relatively unimportant, and a consequence of rather than a driving force for this development.

4.2. *Cloud PV*

In order to determine the source of the low level cyclonic PV maximum, in this section we consider trajectories between 00 and 21 UTC on 2 August, which finish 1, 2, 3 and 4 km above the point marked by a "P" in Fig. 11. A region of anomalously cyclonic PV at 1 km, in the shape of a comet with a head just northwest of the surface low and a trailing tail along the warm side of the associated cold front, is shown in Fig. 13 at 21 UTC 2 August. The minimum PV in the head is about −3 PVU, which is considerably lower than typical tropospheric values which are usually above −1.5 PVU (HMR). The position of the cloud at this level can be estimated from the shading, with medium indicating relative humidity less than 80%, light between 80% and 90% and white greater than 90%. The origin of this saturated air with anomalously cyclonic PV is

Fig. 13. RAMS model 21-h forecast verifying at 21 UTC 2 August 1990. PV field at 1 km, contours every 0.5 PVU, with relative humidity, medium shading less than 80%, light shading between 80% and 90% and white greater than 90%.

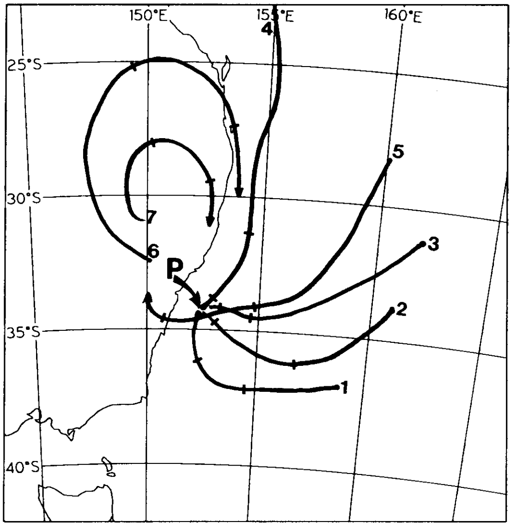

Fig. 14. Mid-upper level trajectories derived from the RAMS model between 00 and 21 UTC on 2 August 1990. Trajectories start at the corresponding number given in Tables 4 and 5, with crosses indicating 12 and 18 UTC times. Trajectories 1, 2, 3 and 4 finish 1, 2, 3 and 4 km respectively above the centre of the low level PV anomaly marked P.

shown by trajectories 1, 2, 3 and 4 in Fig. 14, with corresponding values of height, relative humidity, potential temperature, pseudo wet bulb potential temperature, potential vorticity and vertical velocity in Table 4.

The air is originating in the boundary layer on the warm side of the cold front. The variables in Table 4 corresponding to trajectory 1 indicate rapid ascent only in the last 2 h during which the parcel rose by 1 km. It was not until the onset of condensational heating, associated with the rapid rise of saturated air, that the parcel acquired a large negative PV value. The generation of PV by vertical gradients of latent heating can be understood from the equation (HMR) for the time rate of change of PV due to change in θ:

$$\frac{\mathrm{d}P}{\mathrm{d}t}=\frac{1}{\rho}\,(\xi_{\mathrm{a}}\cdot\nabla\dot{\theta}).$$

PV is generated by differential heating in the direction of the absolute vorticity vector ξ_{a}. For the scales of motion considered here the vertical components of ξ_{a} and $\nabla\dot{\theta}$, i.e., $\xi_{\mathrm{a}}\,\partial\dot{\theta}/\partial z$, will dominate

Table 4. *Values of h, RH, θ, θ_e, PV and w along the low level trajectories in Fig. 14 (units are km, %, °K, °C, PVU and m s^{-1}, respectively)*

No.	Time	h	RH	θ	θ_e	PV	w
1	00/2	0.25	86.3	290.0	14.9	−0.34	+0.00
	06/2	0.23	85.6	288.5	13.6	−0.23	+0.00
	12/2	0.17	84.0	288.6	13.5	−0.14	+0.00
	15/2	0.13	87.5	288.7	14.0	−0.20	+0.00
	18/2	0.13	94.4	289.0	14.8	−0.37	+0.00
	19/2	0.13	96.0	289.5	15.3	−0.44	+0.01
	20/2	0.47	99.5	290.8	15.1	−2.12	+0.16
	21/2	1.00	99.8	292.9	15.1	−2.88	+0.19
2	00/2	0.26	87.3	290.5	15.5	−0.17	+0.00
	06/2	0.26	89.8	289.5	14.8	−0.22	+0.00
	12/2	0.26	88.4	289.2	14.1	−0.20	+0.00
	15/2	0.17	93.4	289.5	15.0	−0.29	+0.00
	18/2	0.73	99.8	292.5	15.8	−1.98	+0.17
	19/2	1.33	99.9	295.2	15.9	−2.43	+0.29
	20/2	1.84	99.3	297.4	15.5	−1.92	+0.18
	21/2	2.00	98.7	298.0	15.1	−1.54	+0.09
3	00/2	0.23	91.7	290.2	15.9	−0.14	+0.00
	06/2	0.26	88.3	290.2	15.2	−0.17	+0.00
	12/2	0.34	90.9	289.2	13.9	−0.25	+0.01
	15/2	1.11	99.3	291.9	13.7	−1.21	+0.13
	18/2	2.82	98.5	300.3	14.6	−1.05	+0.20
	19/2	2.95	97.8	301.2	14.8	−1.01	+0.17
	20/2	2.95	96.4	301.6	14.9	−1.09	+0.10
	21/2	3.00	88.5	302.0	14.4	−1.17	+0.02
4	00/2	2.05	96.4	299.1	16.1	−0.45	+0.01
	06/2	2.44	87.1	298.4	13.5	−0.36	−0.01
	12/2	2.73	98.9	301.0	15.0	−0.98	+0.08
	15/2	3.63	94.2	303.6	14.4	−1.27	−0.04
	18/2	3.84	95.6	303.9	13.9	−0.79	+0.07
	19/2	3.93	95.7	304.3	13.9	−0.72	+0.08
	20/2	4.02	94.4	305.0	14.0	−0.72	+0.10
	21/2	4.00	82.7	305.3	13.6	−0.85	−0.01

the PV production. It is evident from this equation that above the level of maximum heating the vertical heating gradient reverses sign and so does the PV generation. If we assume the latent heating is proportional to the vertical velocity in saturated air then parcels gain cyclonic (anticyclonic) PV below (above) the level of maximum vertical velocity. In keeping with this result continuation of trajectory 1 to 03 UTC 3 August (not shown) indicated that this air continued to rise to about 3 km, with PV returning to typical tropospheric values. Strictly we should include friction in the PV production equation, but like RSK we do not yet have model derived PV diagnostics. An

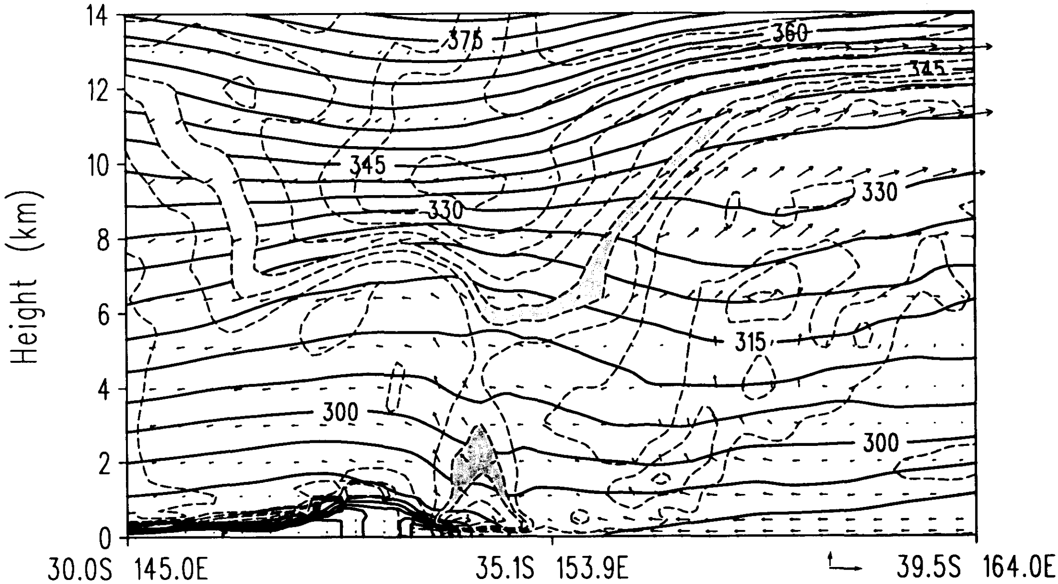

Fig. 15. Cross section along the line AB in Fig. 13, of PV, θ and wind vectors in the plane of the section from a 21-h RAMS model forecast verifying at 21 UTC 2 August 1990. PV contours are every 0.5 PVU with shading between -1.5 and -2.0 PVU. θ contours are every 5°K and the horizontal (vertical) vector below the section corresponds to 65 (0.3) m s^{-1}.

approximate calculation of model PV generation based on vertical velocities and saturated specific humidities in the region of interest indicates values as high as 2 PVU/h are achieved. RSK for their storm indicate that friction effects are smaller but we cannot be sure of that here.

The basic ingredients of a normal mode as suggested in Snyder and Lindzen (1991) can be seen in a cross section along the path of the storm in Fig. 15 looking from south to north. There is a basic state *N/S* temperature gradient with warmer air to the south, implying (through thermal wind balance) an increasing easterly wind with height. The PV of the perturbation slopes slightly eastward with height, enabling it to draw energy from this basic state. The perturbation propagates westward implying a steering level and maximum vertical velocity at about 1.5 km. Below this level the upward vertical motion is in phase with but just to the west of the cyclonic low level PV perturbation, amplifying the mode and resisting the tendency for the mean flow to shear it to the east. Above this level the vertical motion slopes significantly westward with height to be in phase with but just east of the anticyclonic component of the PV perturbation, again amplifying the mode but this time resisting the tendency for the mean flow to shear it to the west. All the ingredients of an unstable mode (as described in HMR) are present but with the source of the perturbation PV the vertical gradient of the latent heating rather than the *N/S* PV gradient of the basic state. A schematic diagram illustrating these features was given in Fig. 3b.

Trajectories 2 and 3, ending at 2 and 3 km respectively above the PV anomaly at 21 UTC, illustrate how PV propagates along the front like a wave. Cyclonic PV is continually being created below the steering level in saturated air ascending ahead of the Low and anticyclonic PV is being created above the steering level just behind the High. This amplifies the existing perturbation and prevents it being torn apart by the basic shear. PV is not conserved along any of these trajectories clearly showing the importance of diabatic processes. This is further supported by comparing model runs with and without the effects of latent heating. Compared to the 13 hPa deepening in 12-h for the full physics run, turning off the latent heating slows down the propagation of the second phase of the development and the surface pressure drops by just 6 hPa as shown in Table 3.

Trajectory 4, ending at 4 km above the PV anomaly at 21 UTC marks a separation between the PV being produced diabatically below and that advected from stratospheric sources above. Along this trajectory the PV changes relatively little.

4.3. Upper level PV

The origin of the unsaturated air with anomalously cyclonic PV at upper levels (above 6 km) is shown by trajectories 6 and 7 in Fig. 14, with corresponding values of height, relative humidity, potential temperature, pseudo wet bulb potential temperature, potential vorticity and vertical velocity in Table 5. Clearly the air is recirculating inside the isolated PV vortex, with near horizontal trajectories, and very good conservation of all quantities. Note again the change in PV (and in several of the other fields) over the 1st 12 h is due to nudging the model tendencies towards the ECMWF values. As stated before this was used as a form of initialisation. Once the nudging is turned off the conservation is very good.

Table 5. *Values of h, RH, θ, θ_e, PV and w along the mid-upper level trajectories in Fig. 14 (units are km, %, °K, °C, PVU and m s^{-1}, respectively)*

No.	Time	h	RH	θ	θ_e	PV	w
5	00/2	0.23	92.6	293.9	19.6	−0.04	+0.00
	06/2	0.73	94.1	294.3	17.2	−0.66	+0.02
	12/2	2.22	99.9	298.7	15.3	−1.25	+0.14
	15/2	4.06	98.0	306.7	15.3	−1.10	+0.21
	18/2	5.72	92.2	312.3	15.2	−0.72	+0.08
	19/2	5.94	88.5	313.0	15.2	−0.80	+0.04
	20/2	6.02	86.3	313.2	15.1	−0.74	+0.01
	21/2	6.00	86.0	313.2	15.1	−0.82	−0.01
6	00/2	6.36	32.8	309.7	12.4	−1.51	+0.00
	06/2	6.58	25.1	311.6	12.8	−2.62	−0.00
	12/2	6.45	25.2	314.1	13.8	−3.59	−0.00
	15/2	6.06	23.0	312.2	13.2	−3.27	−0.02
	18/2	6.02	25.0	312.2	13.2	−3.39	−0.00
	19/2	6.02	25.5	312.3	13.2	−3.49	+0.00
	20/2	6.02	25.3	312.5	13.3	−3.53	−0.00
	21/2	6.02	25.7	312.2	13.2	−3.57	+0.00
7	00/2	7.13	11.1	313.8	12.9	−5.44	+0.00
	06/2	7.39	7.3	318.5	14.4	−5.48	+0.01
	12/2	8.37	12.0	332.3	18.9	−7.78	+0.08
	15/2	8.33	13.1	331.4	18.7	−7.89	−0.01
	18/2	8.11	14.8	329.5	18.3	−7.59	−0.02
	19/2	8.11	14.0	330.0	18.4	−7.42	−0.02
	20/2	8.07	15.0	329.6	18.3	−7.23	−0.01
	21/2	8.07	15.3	329.7	18.3	−7.18	−0.01

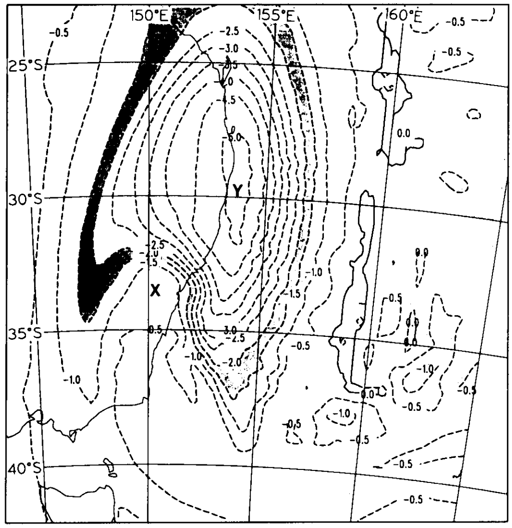

Fig. 16. RAMS model 21-h forecast of the PV field at 6 km, verifying at 21 UTC 2 August 1990. Contours every 0.5 PVU, with X and Y marking the termination points of trajectories 5 and 6 respectively.

Trajectory 5 shows air parcels originating in the boundary layer, increasing their potential temperature by absorbing latent heat as they rise through the atmosphere to about 6 km. PV increases below the level of maximum vertical velocity ($\sim$4 km) and decreases above since the air remains near saturated throughout most of this trajectory. Latent heating is thus a mechanism for getting air of less than 1 PVU from isentropic level 293 to 313, a gain of some 20°K. Fig. 16 indicates that the erosion of the PV in the upper level vortex at the 6 km level is due to this process, since trajectory 5 (marked X) terminates in the middle of this region. This effectively alters the location of the upper PV anomaly and may facilitate the interaction with the low level PV anomaly during the third phase of the storm.

5. Discussion

In this paper, using a "PV thinking" perspective, we have studied the evolution of an intense mesocyclone that developed near the East coast of

Tellus A/47/5:1-19

Australia on 2 August, 1990. Development can be divided into three stages:

Firstly an upper level PV anomaly of stratospheric origin became cut off over eastern Australia. Over a period of several days the low level flow induced by the intense upper level PV anomaly produced a low level cold front. Although the potential temperature contrast across the front was only 5° or so the equivalent potential temperature contrast was some 30°. The area to the north east of Australia was clearly a significant source of moisture, while at this time of the year the Australian continent was a source of relatively cold dry air. Initially the vertical scale of this circulation is the depth of the troposphere (some 8–10 km) and the vertical velocity varies gradually from zero at the surface to a maximum at 4 km and back to near zero at the tropopause, like that of the Eady mode. The actual parcel trajectories form a slanting conveyor belt, like trajectory 5 in Section 4. Production of negative (positive) PV below (above) the level of maximum vertical velocity is initially weak because of the rapid fall off of relative humidity with height. This region is weakly unstable to small perturbations which develop over a day or so and propagate along the front.

Secondly, as the relative humidities increase due to the long upstream trajectories over warm water, upward motion in the associated frontal cloud band leads to more intense latent heating and PV production. The feedback of this PV on the induced vertical motion appears to be to intensify it and confine it to a gradually shallower layer. Eventually the latent heating reaches some threshold, the induced PV anomalies acquire small enough (~ 2 km) vertical separation and the right phase relative to the vertical motion to be self sustaining and propagating in the sense suggested by Snyder and Lindzen (1991) and indicated in Fig. 3. The cross section presented in Fig. 15 supports such a structure for the shallow vortex stage of the 2 August storm simulated here. Energy for growth comes partly from the conversion of basic state potential energy (PE) to perturbation PE and kinetic energy by slantwise convection (baroclinic instability) and partly from latent heating (wave CISK). The horizontal scale of 300–400 km is appropriate for the most unstable mode with a vertical scale of order 2–3 km, following the scaling arguments presented in the introduction.

Thirdly, the low level vortex makes landfall losing its source of moisture and begins to lose intensity. At about the same time the original upper PV anomaly appears to become favourably located relative to another latent heating driven low level PV anomaly. This interaction produces a development with vertical scale of ~ 6 km and horizontal scale of ~ 1200 km.

In answer to the specific questions raised at the start of this study, we found the following:

- No clear role of surface temperature gradients (surrogate PV), in the development of the storm. The surface temperature anomaly never amounted to more than 2°K. Because of this we prefer the wave-CISK mode explanation of the instability presented in Snyder and Lindzen (1991), rather than that of Mak (1994) which suggests the instability is due to interaction between the surrogate PV anomaly at the surface and the PV anomaly at the bottom of the latent heating region. An inversion of the surface PV anomaly is needed to clarify this further.
- Surface fluxes of heat and moisture appeared to play a minor role in the direct development of the storm, affecting the propagation speed and intensity of the second stage low level development by 10%. This was shown by a model run with all surface fluxes turned off. However moisture fluxes are quite large along the warm side of the cold front and may be important for preconditioning the low level environment.
- Crucial dependence of storm development on latent heating, with production (destruction) of PV below (above) the maximum heating level reaching peak values of 2 PVU per hour. Turning off latent heating, reduced storm deepening from 13 hPa to 6 hPa in 12 h.
- At the time of intensification of the shallow mode during the second stage of the storm development, heating rates of up to 400 K per day in the model diagnostics. Perhaps there is some heating rate threshold above which these shallow modes can exist independently of, or in spite of, the upper level PV anomaly.
- The upper level anomaly set up the initial low level thermal and vertical motion fields, which extended over the depth of the troposphere with maximum amplitude (and hence heating) at about 4 km. During the second stage this maximum heating was at about 1.5 km and the upper level PV anomaly did not appear to play a direct role in

the development. An important question seems to be what causes this change in the level of maximum heating (or effectively vertical velocity). We suggest the deeper circulation of the first stage is the balanced response to the upper PV anomaly (the so called "vacuum cleaner" of HMR), whereas the more confined circulation of stage two is attributable to the latent heating itself. In order to quantify these interactions we really need to invert the PV, or solve an omega equation.

• We have produced evidence that the shallow second stage development is an example of the wave-CISK mode of Snyder and Lindzen (1991), with the feedbacks shown in Fig. 3. However it is also clear from trajectory 5 of Fig. 14 that latent heating is an important mechanism for destroying PV at upper levels. This appears to be a far more effective way of modifying PV anomalies (time scale of several hours) than advection of stratospheric air (time scale of several days). This must have implications for processes like downstream development, and production of anticyclonic PV at upper levels in "Blocking" highs.

The storm development presented here is not typical of all Tasman Sea cyclones, although it has many common features. This one is characterised by a slow moving, isolated upper PV anomaly, and was chosen in order to limit the effects of lack of detailed initial data in this region. Many storms develop under an upper level PV anomaly with rapid eastward movement. It is our impression that PV anomalies due to surface temperature gradients do not generally play an important role in Tasman Sea developments, whereas PV anomalies due to latent heating do, although not usually (15%) to produce the shallow wave-CISK mode of this study.

We plan to look at several further cases of cyclones developing in the Tasman Sea, quantifying the roles of different components of the PV. We will supplement the trajectory calculations in this study by using a method of PV inversion like the one described in Davis and Emanuel (1991) and solving an omega equation, including the effects of latent heating, for the vertical velocity. Because of the important role of latent heating in this storm development we expect some sensitivity to the initial moisture fields. In future work we will consider the impact of supplementing the initial fields with locally derived satellite moisture data.

6. Acknowledgements

We thank ECMWF for kindly supplying the data for this study. The RAMS model was run under license from ASTER, Fort Colins, Colorado with assistance from Craig Trenback. The VIS5D program was obtained from the University of Wisconsin, Madison. Jim McGregor of Victoria University, Wellington kindly supplied the satellite picture in Fig. 8. The tephigram in Fig. 9 was drafted from data kindly supplied by Graham Mills and Geof Feren of the Australian Bureau of Meteorology. Comments by Mark Sinclair, Warren Gray, Erick Brenstrum and an anonymous reviewer helped improve the manuscript. This work was supported by the New Zealand foundation for research, science and technology under contract CO1227.

REFERENCES

Bretherton, F. P. 1966. Critical layer instability in baroclinic flows. *Quart. J. Roy. Meteor. Soc.* **92**, 325–334.

Charney, J. G. 1947. The dynamics of long waves in a baroclinic westerly current. *J. Meteor.* **4**, 135–163.

Davis, C. A. and Emanuel, K. A. 1991. Potential vorticity diagnostics of cyclogenesis. *Mon. Wea. Rev.* **119**, 1929–1953.

Eady, E. T. 1949. Long waves and cyclone waves. *Tellus* **1**, 33–52.

Eliassen, A. and Kleinschmidt, E. 1957. Chapters IV and V in Dynamic meteorology. *Handbuch der Physik* **48**. Springer Verlag, pp. 112–129.

Emanuel, K. A., Fantini, M. and Thorpe, A. J. 1987. Baroclinic instability in an environment of small stability to slantwise moist convection, Part I. Two dimensional models. *J. Atmos. Sci.* **44**, 1559–1573.

Golding, B. W. and Leslie, L. M. 1993. The impact of resolution and formulation on model simulations of an east coast low. *Aust. Met. Mag.* **42**, 105–116.

Green, J. S. A. 1960. A problem in baroclinic instability. *Quart. J. Roy. Meteor. Soc.* **86**, 237–251.

Hill, H. W. 1980. A case of intense cyclogenesis in the Tasman Sea. *New Zealand J. of Sci.* **23**, 111–127.

Holland, G. J., Lynch, A. H. and Leslie, L. M. 1987. Australian east coast cyclones. Part I: Synoptic overview and case study. *Mon. Wea. Rev.* **115**, 3024–3036.

Hoskins, B. J., McIntyre, M. E. and Robertson, A. W.

1985. On the use and significance of isentropic potential vorticity maps. *Quart. J. Roy. Meteor. Soc.* **111**, 877–946.

Leslie, L. M., Holland, G. J. and Lynch, A. H. 1987. Australian east coast cyclones. Part II: Numerical modelling study. *Mon. Wea. Rev.* **115**, 3037–3053.

Mak, M. 1994. Cyclogenesis in a conditionally unstable moist baroclinic atmosphere. *Tellus* **46A**, 14–33.

Pielke, R. A., Cotton, W. R., Walko, R. L., Tremback, C. J., Lyons, W. A., Grasso, L. D., Nicholls, M. E., Moran, M. D., Wesley, D. A., Lee, T. J. and Copeland, J. H. 1992. A comprehensive meteorological modelling system, RAMS. *Meteor. Atmos. Phys.* **49**, 69–91.

Reed, R. J., Stoelinga, M. T. and Kuo, Y. H. 1992. A model aided study of the origin and evolution of the anomalously high potential vorticity in the inner region of a rapidly deepening marine cyclone. *Mon. Wea. Rev.* **120**, 893–913.

Sinclair, M. R. 1994. An objective cyclone climatology for the southern hemisphere. *Mon. Wea. Rev.* **122**, 2239–2256.

Snyder, C. and Lindzen, R. S. 1991. Quasi-geostrophic wave-CISK in an unbounded baroclinic shear. *J. Atmos. Sci.* **48**, 76–86.